CONSENSUS GII.4 VIRUS LIKE PARTICLES; A VACCINE CANDIDATE BIOPHYSICAL CHARACTERIZATION, STABILIZATION, AND ADJUVANTS BINDING STUDIES

By

ABDULLAH SAAD A. ALABDULKARIM

Submitted to the graduate degree program in Pharmaceutical Chemistry and the Graduate Faculty of the University of Kansas in partial fulfillment of the requirements for the degree of Master of Science.

_____

Dr. C. Russell Middaugh, Chairperson

_____

Dr. David B. Volkin

_____

Dr. Cory J. Berkland

Date Defended: January 20th, 2016

The Thesis Committee for Abdullah Saad A. Alabdulkarim

certifies that this is the approved version of the following thesis:

CONSENSUS GII.4 VIRUS LIKE PARTICLES; A VACCINE CANDIDATE BIOPHYSICAL CHARACTERIZATION, STABILIZATION, AND ADJUVANTS BINDING STUDIES

_____

Dr. C. Russell Middaugh, Chairperson

Date approved: January 20th, 2016

Abstract:

The World Health Organization (WHO) and the United Nations Children's Fund (UNICEF) estimate globally that 1.9 million children under the age of five years old die annually as consequence of diarrhea. Increasing need for hospitalization, which has negative effects on health care sectors, in addition to mortality incidences mark diarrheal related diseases a growing burden on both health care sectors and the global economy. Introducing novel measures to control and avert the spread of diarrheal disease are of paramount importance. Diarrhea is the main symptom in Acute gastroenteritis (AGE) and according to the United States' National Outbreak Reporting System (NORS), viral agents are the dominant precursors of epidemic AGE outbreaks. More than 90% of humans' acute non-bacterial gastroenteritis breakouts worldwide is caused by Noroviruses (NoVs). NoVs of the Caliciviridae family are none enveloped, positive sense, single stranded RNA virus, noncultivable in cell culture, containing three open reading frames (ORF). Expressing NoVs ORF2 in a baculovirus expression system produces empty virus-like particles (VLPs). These VLPs are very similar to the native virus in terms of morphology and antigenicity, yet lacking the genetic material essential for infectivity, making the VLPs a superb candidate for vaccine development. By comparing the capsid sequence of three different NoVs GII.4 strains, consensus GII.4 VLPs were produced as a potential vaccine with the goal of providing a broader protection against AGE. The main objective of this study is to understand the structural behavior of NoVs Consensus GII.4 VLPs, which is to be used as a vaccine. A complement of biophysical techniques has been employed to characterize the physical stability of Noroviruses Consensus GII.4 virus-like particles (VLPs) as a function of temperature and pH. The VLPs' physical stability are characterized by different spectroscopic techniques and the resulting data are used to construct empirical phase diagrams (EPDs) projecting the entire data set in the form of a colored image. These EPDs are used in the development of excipient screening assays to identify potential stabilizers of the VLPs in solution. The identified stabilizers are then subjected to further screening using fluorescence analysis to determine their optimal concentrations and use in combination. The generated data are used to construct binding isotherms for Consensus GII.4 VLP and aluminum salt adjuvants (Alhydrogel® and Adjuphos®). Binding isotherms were also generated for Norwalk VLP (a previously studied vaccine candidate) and aluminum salt adjuvants. Front Face Fluorescence Spectroscopy is used to evaluate the structural changes associated with Consensus GII.4 and Norwalk VLPs when bound to aluminum salt adjuvants.

Acknowledgment:

This study was conducted in the Department of Pharmaceutical Chemistry, School of Pharmacy, at the University of Kansas.

I am most grateful to my supervisor Dr. C. Russell Middaugh for gracing me with the honor of being a graduate student at his laboratory. Also, I would like to thank him for his continuous help, support and brilliant scientific guidance.

Furthermore, I would like to thank Dr. David Volkin, Dr. Sangeeta Joshi, and all the members of The Macromolecule and Vaccine Stabilization Center, whom I had the pleasure of sharing a great scientific experience.

Also, I would like to thank the Government of Saudi Arabia represented by King Saud University for sponsoring me through my graduate studies.

Finally, I would like to express my highest gratitude to my parents, Mr. Saad And Miss. Hussah Alabdulkarim for their endless love and devotion. For both I dedicate this thesis.

Table of Contents

Section-A

Introduction:

In 2008 Black RE, et al estimated that around 1.3 million of the world's children under 5 years old dies from diarrhea.[1] Liu, L., et al 2012 in a systemic analysis showed that 9.9 % of children deaths per year are a result of diarrhea.[2] The (WHO) World Health Organization and the United Nations Children's Fund (UNICEF) project that 1.9 million worldwide deaths of the same age group are related to diarrheal diseases. In comparison to older estimates of 2.5 million deaths related to diarrhea in the 1990s, the above mentioned projections signal an improvement in lowering mortality rates of diarrheal related diseases.[3] However, global diarrheal morbidity comparisons between 1990 and 2013 show much less progress, with an increasing need for hospitalization and negative effects on economies.[4] These deaths and disease incidences are a growing burden on health care sectors as well as the global economy.[5] It is of great importance to introduce new measures to control and prevent the spread of diarrheal disease.

Acute gastroenteritis (AGE) is a globally prominent cause of illness with significant morbidity and mortality.[6] High incidences of morbidity and patient hospitalization demonstrate the impact of the illness in developed countries with AGE outbreaks.[7] AGE is characterized by acute diarrheal episodes in the presence or absence of vomiting. This gastrointestinal (GI) upset is mostly a result of microbial infection. Microbial agents, (viral, bacterial and protozoal), infect the GI primarily through two major mechanisms,

either multiplication in the intestine or by toxin production.[8] The United States' National Outbreak Reporting System (NORS) indicated that viral agents are the dominant precursors of epidemic AGE outbreaks. Until recently rotavirus was the leading cause of AGE in the United States, and it was the main antagonist in the battle against AGE. However, the introduction of successful vaccination products has significantly lowered the incidences of Rotaviruses' related AGE, consequently lowering its risk. The time declining rates in rotavirus associated AGE were clinically observed was associated with a rise in AGE outbreaks of a different virus pathogen, designated Norovirus.[9-13]

Noroviruses (NoVs) cause over 90% (23 million cases/ year in the U.S) of acute non-bacterial gastroenteritis breakouts worldwide in humans. This illness, spread through an oral-fecal route, affects people of all ages in many life setting (such as schools, retirement homes, cruise ships, military bases, etc). Symptoms such as Vomiting, watery diarrhea, and abdominal pain are usually seen after 15-48 hrs of infection with the virus, and they usually last for 12-60 hrs. Although these symptoms are considered to be short-lived and self-contained, they can be life threatening in geriatric and pediatric population as well as in immunocompromised individuals. Only 10 virions are needed to cause infection in a healthy person, which explains the high prevalence of the disease. Noroviruses (NoVs), a major gastrointestinal pathogen, are the primary cause of AGE globally accounting for approximately 20% of reported cases.[14] In 1968 an outbreak occurred in Norwalk, Ohio affecting half of an elementary school's teachers and students with AGE. The culprit behind this epidemic was recognized as a virus and was assigned the name Norwalk virus

(NV). [15,16] Although visualized in 1972, the fact that NV is noncultivable in cell culture hindered its proper classification until 1990. Xi Jin, et al completed a successful genomic characterization of NV and molecular cloning confirmed the classification of NV as a member of the *Caliciviridae* family.[17] NV And Norwalk-Like viruses (NLVs), referred to currently as NoVs, constitute a 27-38 nm particle, nonenveloped, positive sense polyadenylated, single stranded RNA virus of around 7,500 nucleotides that contains three open reading frames (ORF). [18-20] The longest NoVs ORF, ORF1 encodes nonstructural proteins that are imunoreactive in hosts. ORF2 expression in baculovirus infected insect cells yields a protein capsids (VP1) of 58 kD that self-assemble into virus like particles (VLPs). ORF3 encodes a minor structural protein (VP2) of 22.5 kD that is essential for enhancing the expression and conformation of VP1.[20, 21,23] Noroviruses are classified based on their VP1 into five major genogroups GI-GV. It is believed that genogroups GI, GII and GIV are responsible for human infections. Evidence collected in the past 15 years implicate the GII genogroup as a worldwide prevailing cause of sporadic and epidemic AGE. Most genogroups, including GII, are subdivided based on the amino acid sequences of VP1 into different genoclusters or genotypes. Genogroup II (GII) can be divided into more than 20 genotypes. GII genotype 4 (GII.4) is worldwide the major cause of human AGE outbreaks. GII.4 strains evolution with time is behind outbreaks recurrence and presents a major obstacle in implementing intervention and deterrence measures. GII.4 evolves through alteration of the amino acid sequence of VP1.[22-26] NoVs cannot be cultivated in simple cell culture lines; also, no animal model to study the infectivity exists. These problems have hindered the development of an effective vaccine in the past.

Expressing NoVs ORF2 in a baculovirus expression system produces empty VLPs that self-assemble into a T=3 Icosahedral structure. Although these VLPs are very similar to the native virus in terms of morphology and antigenicity, they lack the genetic material essential for infectivity this has suggested the use of NoVs VLPs as a potential vaccine candidate. This protein complex (VLP) is made of 180 monomers that form a 90 dimer arch-like structure. The major component of this capsid is predominantly composed of VP1 and a few copies of a minor capsid protein (VP2). VP1 consists two domains, a shell domain (S-domain) and a protruding domain (P-domain). The S-domain is essential for the formation of the icosahedral structure while the P-domain, which is composed of two subdomains (P1) and (P2), binds to cellular specific receptors and is considered to be the antigenic part of the system. This antigenicity is limited by the high amino acid sequence variability of the VP1-P2 domain among strains of the same genocluster. This is the reason why protection from illness is not necessarily achieved after first time exposure. NoVs are phylogenetically subdivided into five genogroups and further subdivided into many genoclusters with GII.4 as the major source of global outbreaks. By comparing the capsid sequence of three different GII.4 strains, Houston, DenHaag89 and Yerseke38, NoVs consensus GII.4 VLPs were produced as a potential vaccine with the goal of providing a broader protection against AGE.[26-30]

The main objective of this study is to understand the structural behavior of a promising macromolecular entity, NoVs Consensus GII.4 VLPs, which is to be used as a vaccine. Characterization of the physical stability of macromolecules is one of the crucial steps in the preformulation and formulation development of safe and efficacious

vaccines. To achieve this goal, a complement of biophysical techniques has been employed to characterize the physical stability of Noroviruses Consensus GII.4 virus-like particles (VLPs) as a function of temperature and pH. The VLPs' physical stability are characterized by different spectroscopic techniques such as intrinsic and extrinsic fluorescence, circular dichroism, and static light scattering. The resulting data are used to construct empirical phase diagrams (EPDs) that are used to visualize the entire data set in the form of a colored image. These EPDs were then employed for the development of excipient screening assays to identify potential stabilizers of the VLPs in solution. A library of potential excipients was then screened for compounds that prevent the solution aggregation of the potential vaccines under stress conditions of temperature and pH. The identified stabilizers are then subjected to further screening to determine their optimal concentrations and use in combination. The effect of the stabilizers on the conformation of those potential vaccines is determined using fluorescence or CD analysis. The results obtained from the above mentioned experiments facilitated the construction of binding isotherms for Consensus GII.4 VLP as well as a previous studied vaccine candidate Norwalk VLP to aluminum salt adjuvants (Alhydrogel® and Adjuphos®). The structural changes associated with Consensus GII.4 and Norwalk VLPs when bound to aluminum salt adjuvants were also assessed using Front Face Fluorescence Spectroscopy.

Section - B

Biophysical Characterization and stabilization of Consensus G11.4-VLP:

Materials and Methods:

Consensus GII.4 VLPs expression and purification:

By the alignment of the amino acid sequences of VLP capsid proteins for three NoVs GII.4, Houston/TCH186/2002/US (ABY27560), Yerseke38/ 2006/NL (ABL74391), and DenHaag89/2006/NL (ABL74395), the consensus GII.4 VLP amino acid sequence was designed. Consensus GII.4 sequence was encoded in a synthetic DNA fragment optimized for Sf9 (Spodoptera frugiperda) cells. Sf9 cells were supplied by via GeneArt at Regensburg, Germany for the purpose of developing a recombinant baculovirus to express the consensus GII.4 VLPs. of the DNA encoding the GII.4 consensus VLPs was used to infect Sf9 cells and the supernatant was collected after 5 days of infection. A proprietary process employing multiple orthogonal chromatography and ultrafiltration/diafiltration operations was used to yield VLPs with greater than 99%purity.[31]

Sample preparation:

Recombinantly expressed Consensus G11.4 VLPs (Lot number Ligo 277.003.1, 1.4mg/ml) were provided by Ligocyte Pharmaceuticals a liquid form at 4^{o}C. All

chemicals were purchased from either Fisher Scientific (Pittsburgh, PA) or Sigma (St. Louis, MO) and were of analytical grade.

The VLPs were dialyzed overnight at 4^{o}C against 20 mM Citrate Phosphate buffer containing 150 mM NaCl at different pH values ranging from 3-8 at one pH unit intervals. The buffer exchange was done using Spectra/pro molecular porous membrane tubes (Spectrum Lab, Rancho Dominguez, CA) with a MWCO (molecular weight cut-off) of 15 kD. The protein concentrations of the VLPs were determined by measuring the absorbance at 280 nm using an extinction coefficient of 0.921 ml mg^{-1} cm^{-1} (obtained from the Protparam program in the Expasy server), and the amino acid sequence was provided by LigoCyte (Figure 1). The CD studies were performed at a protein concentration of 0.22 mg/ml. For all other studies a protein concentration of 0.055 mg/ml was employed. All experiments were conducted in duplicate unless otherwise stated.

Methods:

Far-UV Circular Dichroism (CD) Spectroscopy:

The spectral measurements were performed using a Jasco J-810 spectropolarimeter (Tokyo, Japan) with a six-position cell holder attached to a Peltier temperature controller. The CD measurements were performed at a scan rate of 20nm/min over a wavelength range of 200-260 nm with a two second response period and an accumulation of three

using 0.1 cm path-length cuvettes. Thermal unfolding of the VLPs was monitored at 208 nm over a temperature range of 10-85°C at 2.5°C intervals with a temperature ramp rate of 15°C /hour.

Intrinsic Tryptophan Fluorescence Spectroscopy and Static Light Scattering (SLS):

The intrinsic tryptophan fluorescence and static light scattering data were acquired using a PTI (Photon Technology International) Quantamaster spectrofluorometer (Birmingham, NJ) equipped with a turreted four-position peltier-controlled cell holder. The excitation wavelength was set at 295 nm (> 95% Trp emission) and tryptophan emission spectra were acquired at wavelengths ranging from 310-400 nm with a scan rate of 1 nm/sec. The excitation and emission slit width were set at 4 nm for both. Light scattering spectra were recorded at 295 nm by using a second photomultiplier positioned at 180° to the emission detector, and the slit width was set at 1 nm. A temperature ramp of 10-85 °C was used with spectra obtained at intervals of 2.5°C with a three-minute equilibrium period between acquisitions. Buffer base lines were subtracted from each spectrum prior to data analysis. Data was analyzed using Fleix™ (PTI) and Microcal Origin 7.0 software. The peak positions and fluorescence intensity changes were obtained using a "center of spectral mass" method. Thus, the reported values are 10-12 nm higher than the actual values and do not correspond to actual peak positions, but accurately reflect changes in peak position values.

Extrinsic (ANS) Fluorescence Spectroscopy:

8-Anilino-1-naphthalene sulfonate (ANS) was used as an extrinsic fluorescent probe to determine surface-exposed hydrophobic patches during the thermal unfolding process of the VLPs. Samples prepared by mixing a 15-fold molar excess of ANS to the VLPs were excited at 385 nm and the emission spectra were acquired from 425-550 nm with a scan rate of 1nm/sec using the same spectrofluorometer described above. Emission spectra were acquired over a temperature range of 10-85 C° at 2.5 C° intervals using a 3 min equilibrium period. Buffer base lines were subtracted from each spectrum prior to data analysis. The methods used for the analysis of ANS spectra were similar to those employed in the analysis of the intrinsic fluorescence data.

Empirical Phase Diagram (EPD):

An empirical phase diagram was created employing data generated from intrinsic tryptophan fluorescence intensity changes and peak position shifts, extrinsic ANS fluorescence intensity changes, CD ellipticity values at 208 nm and static light scattering. Briefly, the data is represented as a vector field in a temperature and pH plane, from which a density matrix is generated. Eigenvalues and eigenvectors are calculated based on this density matrix. Eigenvectors corresponding to the three largest eigenvalues are used to transform the vector field into a three dimensional coordinate system, which is then represented as a color map. The dominant eigenvalues are assigned the colors red,

green and blue. The goal of this technique is to detect the changes in color, which present a qualitative picture of the transitional states in the protein. The phase diagram was generated using Matlab software (Mathworks, Inc., Natick, MA).[32,33]

Excipient Screening Method Development:

Based on the results acquired by the above mentioned techniques, a high throughput aggregation assay was developed by monitoring the scattering of 0.1 mg/ml Consensus VLP at 350 nm (in a Cary 100 UV-Visible Spectrophotometer) over a period of 1 hr at 60^{o}C in 20 mM Histidine buffer, pH 6.5 containing 150 mM NaCl. A library of Generally Regarded As Safe (GRAS) excipients were then screened to detect potential stabilizers. The potential candidates were established based on their abilities to inhibit VLPs aggregation. The percentage of inhibition of aggregation in presence of excipients is calculated using the following equation:

$$\% \text{ inhibition of Aggregation} = \frac{A_{350}^{\text{VLP alone}} - A_{350}^{\text{VLPs+excipient(s)}}}{A_{350}^{\text{VLP alone}}} * 100$$

where $A_{350}^{\text{VLP alone}}$ and $A_{350}^{\text{VLP+excipient}}$ is the OD_{350} values at 1 h of the Consensus VLP in the absence and presence of selected excipients, respectively.

Results:

Far-UV Circular Dichroism Spectroscopy:

Changes in the secondary structure of Consensus GII.4 VLPs were followed by monitoring the changes in CD spectra across pH intervals ranging from 3-8, and a temperature gradient of 10-85 ^{o}C. Figure 2A shows The CD spectra obtained at 10 ^{o}C for the studied pH intervals. All pH ranges display a single minimum around 208 nm and a detectable transition (shoulder) at 230 nm. Figure 2B shows the effect of temperature on consensuses GII.4 VLPs secondary structure. The thermal denaturation acquired by CD melts indicate loss of secondary structure at different pH intervals. At pH 3, the CD melt of the consensus VLP reveals a thermal transition (Tm) at 73 ^{o}C. At pH 4 and 5, Tms were observed to be at 75 ^{o}C; whereas at pH 6 a 79 ^{o}C was obtained. Thermal transitions were not resolved for pH 7 and 8, where no marked transitions were detected (Table 1).

Intrinsic Fluorescence Spectroscopy:

Tertiary structure conformational alterations were monitored by following the changes in both Tryptophan peak positions and Tryptophan fluorescence intensity as a function of temperature and pH (Figure 3A and 3B). Tryptophan residues buried in the hydrophobic core are seen to emit absorbed light at a maximum of 330. As the

macromolecule denaturates thermally the buried tryptophan residues will be more exposed to a hydrophilic (aqueous) environment as the protein unfolds. This hydrophilic exposure will shift the peak position to higher weave lengths, known as a red shift. This red shift can act as an indicator for the loss tertiary structure as the macromolecule unfolds. Figure 3A shows results for the pH range of 3 to 8 with the earliest transitions having Tms of 55 ^{o}C and 57 ^{o}C at pH. 3 and 8 respectively. At pH 5 and 6 the VLP resists unfolding with late transitions and Tms of around 64 ^{o}C. In contrast, at pH 4 and 7 the consensus VLPs displayed similarity in both transition and Tms (61 ^{o}C). Alteration to the tertiary structure can also be monitored using the temperature-dependent tryptophan fluorescence intensity changes (figure 3B). At pH 5 and 6, consensus VLPs show a transition onset at 60 ^{o}C. The onset of transitions for both pH 3 and pH 4 is at 55 ^{o}C and 57 ^{o}C, respectfully. A broader transition is observed for both pH 7 and pH 8 which starts at around 55 ^{o}C.

Static Light Scattering:

The aggregation behavior of the consensus GII.4 VLP was studied by monitoring static light scattering (SLS) data at 295 nm (figure 4). The onset and extent of aggregation are shown to be pH dependent, with both pH 7 and 8 displaying different aggregation profiles than the rest of the pH values. The extent of aggregation is seen to be maximum at pH 3 with an aggregation onset of 55 ^{o}C, whereas the aggregation onset for pH values of 4, 5 and 6 are 58, 56, and 62 ^{o}C respectively (Table 3).

Extrinsic Fluorescence Spectroscopy:

The changes in the fluorescence intensity of ANS bound to the VLPs as a function of pH and temperature are shown in Figure 5. At all pH values, the fluorescence intensity is initially high at low temperatures and then gradually decreases with some sharp transitions. As evident from the figure, Consensus VLPs show a single transition around 55^{o}C at pH 3, but at pH 6 and 7 the VLPs exhibit two distinct transitions, a first transition around 25-30^{o}C and a second one around 63-67^{o}C, respectively. Double transitions also occur at pH 8; however, the minor transition occurs at a higher temperature (at 50^{o}C). At pH 4 and 5, the first transition is barely visible.

Empirical Phase diagram (EPD):

An empirical phase diagram was constructed (Figure 6) using the data generated from CD melts, intrinsic tryptophan fluorescence intensity changes, changes in the tryptophan emission maxima, ANS fluorescence intensity changes and static light scattering as a function of pH and temperature. Several phases in the EPD are apparent and marked as regions P1-P7. Regions of uniform color indicate defined structural states while sudden changes in color represent alterations in the physical state of the VLPs.

Excipient screening:

Aggregation was one of the most obvious mechanisms of consensus GII.4 VLP degradation and therefore an aggregation based turbidity assay was developed to screen for potential stabilizers. Based on the data generated using the above-mentioned techniques, a general idea about the pH and temperature boundaries at which the VLP is most stable is established. An aggregation-based assay to screen a library of Generally Regarded As Safe (GRAS) excipients that might be used to increase VLP stability was developed. Experiments were carried out in histidine buffer (20 mM Histidine at pH 6.5 containing 150 mM NaCl). Figures 7A and 7B show representative aggregation profiles of the Consensus GII.4 VLP in the absence and presence of selected excipients, where the aggregation of the VLP is inhibited or accelerated over a period of 1 hour. The percentage of inhibition of aggregation is calculated from the equation described in the materials and methods section.

From the data (Table 4), it is evident that sodium citrate (0.2M), trehalose (20%), dextrose (20%), glycerol (15%), lysine (0.3M), sucrose (20%) and mannitol (10%) inhibit the aggregation of the VLPs by more than 90%. Albumin, ascorbic acid and gelatin caused immediate turbidity when added to the VLP solution and thus could not be used in this assay. Some other excipients (e.g. glutamic acid, glycine and malic acid) also showed promising results; however, the excipients which showed more than 90% protection of aggregation were selected to further monitor the potential conformational changes associated with the VLP as a function of temperature. Although sodium citrate and lysine were good inhibitory candidates, they decreased the T_m of the peak position shift (data

not shown). Therefore, glycerol, sucrose and mannitol at different concentrations and combinations were examined for use in a preliminary formulation of the VLP as a result of both aggregation inhibition and enhanced conformational stability.

Optimization of Excipient Concentrations and Combinations:

Promising candidates for VLP stabilization were chosen based on the preliminary screening assays described above. The optimal concentration of these potential stabilizers and their influence on VLP conformational stability were determined. The goal of this approach was to find an optimized recipe that will suppress Consensus GII.4 VLP structural deformation to a maximum. To achieve this, conformational changes of the VLP (0.055mg/ml) were monitored in histidine buffer (20mM Histidine buffer, pH 6.5, 150 mM NaCl) by using intrinsic tryptophan fluorescence spectroscopy. Red shifts in the tryptophan emission maxima indicate increased unfolding (destabilization) of proteins in the VLP. The goal is to delay such shifts to a higher temperature (higher Tm). Figures 8A and 8B show plots of tryptophan peak position changes as a function of temperature of Consensus VLP in the presence of different concentrations and combinations of selected excipients. Table 5 shows the shifts in the T_m values of Consensus VLP in presence of the excipients (at different combinations and concentrations). The maximum change in the midpoint of the thermal transition (T_m) was seen with the combination of 10% sucrose and 15% mannitol (T_m shifts from 65.5 °C to 69.27 °C). 20% mannitol is the second best candidate and increased the T_m value by 2.9°C. Also, an additive effect is seen when using the combination of 10% sucrose and 10% mannitol (T_m shifts of +2.5 °C). Other

excipients alone or in combination showed minimal shifts or no shifts at all in the T_m values.

Discussion:

The physiochemical properties of Consensus GII.4 VLPs were examined using multiple biophysical techniques to characterize the stability of the macromolecule complex as a function of pH and temperature. Circular dichroism (CD) studies performed on the VLPs provided insight into the protein's secondary structure. CD spectra obtained at 10 ^{o}C at different pH intervals showed a single minimum around 208 nm and a lassei transition (shoulder) at 230 nm, suggesting a class II beta-protein (single minimum 208nm) and a type I beta turn conformation (shoulder at 230nm), a conformation adapted by many compact macromolecules (figure 2A).[34-37]In comparison, *Ausar, SF, et al*[38] study of a NV vaccine also found ClassII beta-protein in this vaccine candidate. CD Temperature perturbation studies show in figure 2B a loss in secondary structure for the VLPs at pH intervals 3-6. Over these ranges the sharp thermal transitions is clear evidence for the unfolding of the macromolecule when it exceeds 70 ^{o}C with pH 3 showing the earliest onset and pH 6 as the least. This is in contrast to data suggesting Norwalk VLPs are more stable in an acidic environment. This acid stability presumably reflects viral resilience to the pH.[39] Transition midpoint (Tm) values for the Consensus GII.4 VLP were calculated across the different pH conditions tested finding the VLP to be most resistance to temperature induced unfolding at pH 6. However, the pH from 7 to

8 showed no marked transitions. In comparison, *Ausar, SF, et al*, suggested that the NV VLPs capsid undergoes disruption at basic pH conditions, a phenomenon observed by *White et al*, as well.[38,39] This may indicate that Consensus VLPs behave similarly in basic pH conditions, explaining the absence of any phase transition in pH 7 and 8.

According to the amino acid sequence shown in Figure 1, Consensus GII.4 VLP has 6 tryptophan residues. Fluorescence studies of tryptophan peak position changes (figure3) illustrate the effect of pH and temperature on the tertiary structure of Consensus VLPs. Shifts in peak position from lower to higher wavelengths (red shift) are a clear indication of the change in polarity of the environment surrounding tryptophan residues. Tryptophan residues emitting light at wavelength values close to 330nm suggest tryptophans that are on average buried in apolar regions of the protein. Changes in environmental polarity toward hydrophilicity as a result of structural perturbation will yield a red shift in peak position as seen in figure 3A. The earliest red shift is demonstrated in pH ranges 3 and 8, suggesting that Consensus VLPs tertiary structure is most fragile at those pH conditions. The most resistant to tertiary structure dismantling are seen with pH conditions 5 and 6, where the Tm for both is around 64 ^{o}C (Table 3), corroborating the results obtained with CD. Alterations in the tertiary structure were further studied by monitoring tryptophan fluorescence intensity changes (figure 2B). The delayed onset displayed in pH conditions 5 and 6 supports fluorescence peak position data discussed above. Also, tryptophan weak fluorescence intensity changes observed at pH 7 and 8 are evidence for disruption of consensus VLP capsid in basic pH conditions.[41]

ANS (8-Anilino-1-naphthalene sulfonate) is a hydrophobic probe used to monitor the presence of accessible hydrophobic patches in a protein. The fluorescence intensity of ANS is very weak in aqueous solutions, but when bound to hydrophobic surfaces (such as in structurally disrupted proteins), the ANS fluorescence intensity increases drastically. Exploiting this phenomena, more information regarding the protein's tertiary structure conformation is attained. In Figure 5, a greater intensity observed in all pH ranges at 10ºC indicate ANS bound to hydrophobic regions of the macromolecule complex. A single early transition observed at pH 3 supporting previous results indicating the instability of NV VLP at this pH. At pH 4 two transitions are displayed. First, a minor transition starting at 26ºC and a second at 65ºC. Similar transitions are also observed at pH 5. More pronounced transitions are detected at pH 6 and 7 with an initial transition at around 30ºC and a second near 62ºC. The early transition observed in pH intervals 4-7 are probably a result of the unfolding of one of the two domains on the VLPs capsid. A similar result was seen in NV VLPs' *Ausar, SF, et al* [38] study.

Data obtained from Static Light Scattering showed that both the onset temperature and extent of aggregation are pH dependent (Figure 4). The highest extent of aggregation is seen in pH 3 with an early onset, backing up our initial estimate of the instability in this pH range. Both pH 4 and 5 displayed similarity in onset temperature; however, pH 5 shows a different behavior evinced by the lag in the intensity curve. This may be attributed to a resistance to temperature induced aggregation. The latest onset is observed at pH 6, supportive of our previous data in that the maximum resistance to structural

conformational changes for Consensus GII.4 VLPs occurs under pH 5-6 conditions. The descending curves (figure 4) for pH conditions 7 and 8 may indicate a sudden precipitation of the VLPs at the onset temperature (Table 3), more evidence of instability of the VLPs in basic pH conditions.

The construction of the empirical phase diagram (EPD) illustrates a variety of alterations in the consensus GII.4 VLPs physical state (Figure 6). The changes in the conformational and colloidal stabilities as a function of pH and temperature was qualitatively described by changes in color. Throughout the EPD, the different conformational states the VLP adopts are depicted over different regions (labeled from P1 to P7). The region in greenish yellow (P1 and P4) are the regions of maximum stability in which the VLP remains in its native, folded conformation. Regions P3 and P5 colored in light green are the regions where the VLP exhibits perturbed tertiary structure. Regions labeled as P6 may reflect molten globule-like states of the VLPs. Phases P2 and P7 are the regions of minimum stability with extensively aggregated and perturbed secondary and tertiary structures. The VLP seems to be extensively unfolded in Phase P2.

The aggregation behavior obtained from excipient screening assays (Table 4) found that amino acid, sugars, and carbohydrates stabilize consensus GII.4 VLPs; similar results were demonstrated by *Kissmann J, et al*.[40] Exclusion of lysine and sodium citrate from further investigation is due to their negative effect on the conformational stability of consensus GII.4 VLPs as shown by tryptophan fluorescence spectroscopy (data not shown). Osmolytes like trehalose, sucrose, and glycerol are known to stabilize

microorganisms naturally in stressful conditions; glycerol presumably enhances the stability by preferential hydration of the native state. Sucrose and terhalose, at elevated concentrations presumably also stabilize liquid formulations through a preferential hydration mechanism as well as hydrogen bond interactions. [41-43,45] Mannitol, often used as a bulking agent is also known to often in stabilize proteins, but in combination with sucrose are often found to be beneficial in stabilizing lyophilized formulations.[46] Glycerol, Sucrose, and mannitol displayed the most favorable outcome in both inhibition of aggregation and increasing T_m values. Thus they were chosen as promising candidate to be used in different combinations to enhance the stability of consensus GII.4 VLPs.

Using different excipient combination to achieve the most favorable outcome in delaying conformational alteration through increasing the $T_{m,}$ value of consensus GII.4 VLPs are displayed in figure 8. Sucrose at high concentrations (15% and 20 %) shows better protection against conformational changes compared to lower values. However, combining 10% sucrose with 15% mannitol displayed the most promising outcome in delaying transition midpoint T_m (Table 5), an additive effect frequently previously observed with protein formulations.[43,44,46]

In conclusion, the physical stability of Consensus G11.4 VLPs was characterized in terms of secondary and tertiary structures as well as its colloidal stability. The thermal stability of Consensus G11.4 VLPs was shown to be pH dependent. Based on these results, it appears that VLPs are most stable around pH 5-6, and below ≈ 60oC. From excipients screening studies, it is shown that the combination of 15% mannitol and 10% sucrose yields VLPs with the highest conformational stability.

Section C

Adsorption of Norwalk and Consensus G11.4 VLPs to Aluminum Salts – Binding isotherm and Front Face Fluorescence Studies

Overview:

Since the introduction of potash alum (aluminum potassium sulphate) by Glenny and coworkers in 1926, Aluminum salts have been vital components of vaccine formulation, especially with those antigens that lack endogenous adjuvants (e.g. VLPs).[47,48] Aluminum salt adjuvants, highly charged molecules, help low potency antigens to elicit a stronger immune response through a variety of proposed mechanisms. For half a century after they were introduced, aluminum salts adjuvants theorized mechanism of action (MOA) was attributed to a depot effect.[49] However, in the last decade many hypotheses have been introduced with regard of their MOA including: activation of the innate immune system and induction of NOD-like receptor (NLR) family, through the pyrin domain containing 3 (NLRP3) inflammasomes among many others. [50-51] A definitive explanation on how these adjuvants stimulate the immune system is yet to be elucidated. The fact that Aluminum hydroxide (Alhydrogel®) and aluminum phosphate (Adjuphos®) possess both high safety and efficacy profiles made them widely used as commercial human vaccine adjuvants.[52] Although contradicted recently[53,54], the main dogma in adjuvant Induction of immune response was thought to be achieved by increasing the adsorption of antigen to the adjuvant surface.[55] Many forces attribute to this adsorption, ranging from electrostatic interaction and hydrogen bonding to van der

Waals forces and hydrophobic interactions between antigens and adjuvants.[56] The objective of this section is to construct binding isotherms of Norwalk-VLPs and Consensus G11.4 VLPs to aluminum salt adjuvants (Alhydrogel® and Adjuphos®) and to monitor structural changes associated with Norwalk and Consensus G11.4 VLP when bound to adjuvants using Front Face Fluorescence Spectroscopy. It is hoped that these results will aid in the final construction of efficacious formulations.

Materials and Methods:

Based on structural characterization studies and the empirical phase diagram reported previously in section A, the buffer of choice for conducting preliminary binding isotherm studies was 10 mM imidazole, pH 7.5 containing 0.15M NaCl. Ligocyte Pharmaceuticals provided both NV-VLPs and Consensus G11.4 VLPs. Stock NV-VLP (Lot 45.06007.1) and Consensus G11.4VLP (Ligo 277.003.1) solutions were used for the binding isotherm studies. For front face fluorescence studies, VLP samples (Lot number NV-VLP M7VP1 and G11.4C Consensus CM3 dated 10Nov08) in 20 mM Histidine buffer, pH 6.5 + 0.15M NaCl were used. Concentrations of the VLPs were determined spectrophotometrically from their respective molar extinction coefficients (280 nm, of 0.852 ml mg-1 cm-1 for NV-VLP and 280 nm, of 0.921 ml mg-1 cm-1 for Consensus G11.4 VLP). Adjuphos (batch number 9039) and Alhydrogel (batch number 4102) manufactured by Brenntag Biosector, Denmark were purchased from E.M. Sergeant Pulp & Chemical Co., Inc., Clifton, NJ. The concentration of stock Adjuphos and Alhydrogel were 4.8 mg/ml and 10.1 mg/ml, respectively.

Construction of Binding isotherms of Norwalk-VLP and Consensus G11.4 VLP to Alhydrogel and Adjuphos:

The binding assay was performed by adding increasing amounts of VLPs to a fixed amount of Alhydrogel (0.5 mg/ml) and Adjuphos (0.5 mg/ml) in 1.5 ml microfuge tubes. The final sample volume in each tube was 200 µl. The samples were mixed by gentle 360^{o} rotation at 4^{o}C for 1 hour and then centrifuged at 14,000 rpm for 1 min. It was found that equilibrium (maximum binding) was reached by this procedure. The amount of unbound VLPs was measured by monitoring the A280 nm of the supernatants. All measurements were done in triplicate.

Front Face Fluorescence Spectroscopy:

Fluorescence spectroscopy employing front face sampling geometry was used to probe changes in the tertiary structure of the VLPs as a function of temperature for both Norwalk and Consensus G11.4 VLP in solution, as well as adsorbed to the aluminum hydroxide adjuvant with and without the excipients selected earlier (section A). For all studies, a VLP concentration of 0.1 mg/ml was used. Sample solutions were prepared in triangular fluorescence quartz cuvettes by combining the aluminum salt (alhydrogel) suspension with an appropriate volume of 20 mM Histidine buffer, pH 6.5 + 0.15M NaCl, such that the final calculated aluminum concentration was 1.7 mg/ml in the absence and presence of 0.1 mg/ml VLP in a total volume of 2 ml. The concentration of

aluminum was determined from the data provided by the supplier in the lot specification sheet.

Samples containing adjuvant were allowed to settle in the cuvettes overnight at 4°C. Emission spectra were recorded from 300 to 400 nm using a spectrofluorometer equipped with a Peltier thermostated cuvette holder (Photon Technologies International, Lawrenceville, NJ) employing an excitation wavelength of 295 nm (>95% Trp emission). Data were collected every 1 nm at a scanning rate of 1 nm/s. Emission spectra were obtained every 2.5 °C from 10 to 85°C with 300 seconds of thermal equilibration at each temperature. The data were processed using Origin version 7.0 software. A buffer baseline was subtracted from each raw emission spectrum.

Peak positions of the emission spectra were obtained using a "center of spectral mass" method (described in section A) using Origin 7.0 software. The actual peak positions are approximately 10-14 nm shifted from their actual values but the method does accurately reflect changes in the peak positions.

Results and discussion:

Binding isotherms of Norwalk-VLP and Consensus G11.4 VLP to Alhydrogel and Adjuphos:

Binding isotherm plots of VLP concentration with Alhydrogel are shown in Figure 9A. It is evident that both NV-VLP as well as Consensus VLP bind tightly to Alhydrogel. In the case of the consensus VLP, saturation began to be approached after 0.8 mg/ml but was not reached saturation was also not obtained for NV-. For the NV-VLP, saturation

was not obtained because the stock concentration of NV-VLP was 1.07 mg/ml and thus measurements could not be carried out beyond 1.0 mg/ml. Under the conditions examined by us, both NV-VLP and Consensus VLP were strongly bound to the Aluminum hydroxide adjuvant.

Adsorption isotherms of NV-VLP and Consensus-VLP to Adjuphos do not show any appreciable binding as shown in the plots (Figure 9B). NV-VLP and Consensus G11.4 VLP have theoretical acidic pI values of 5.64 and 5.61, respectively (determined from the Expasy Protparam server). Alhydrogel, being a basic particulate salt with a point of zero charge of 11 was shown to have a stronger binding affinity for both of the VLPs than Adjuphos.[57] This suggests that electrostatic interactions may play a significant role in adsorption of the VLPs to the surface of aluminum hydroxide.

Since both the VLPs bind alhydrogel strongly, the extent of tertiary structural changes associated with Norwalk and Consensus G11.4 VLP when adsorbed to alhydrogel was monitored.

Structural changes associated with Norwalk and Consensus G11.4 VLP when bound to Alhydrogel using Front Face Fluorescence Spectroscopy:

Shown in Figures 10A and B are the tertiary structural changes as determined by front face fluorescence spectroscopy for the Norwalk and Consensus G11.4 VLPs alone and when adsorbed to Alhydrogel in the absence and presence of stabilizers. Figure 10(A) shows that at 10^{o}C the tryptophan peak position of NV-VLP is approximately 342

nm (as calculated by the center of spectral mass method). With increases in temperature, the peak position gradually increases manifesting a transition midpoint (Tm) around 64^{o}C. In the presence of alhydrogel, although the initial peak position appeared to be slightly higher at low temperatures (344 nm) compared to that of NV-VLP alone, the Tm values are approximately 4-5^{o}C greater in presence of alhydrogel ± selected excipients. Consensus G11.4 VLPs appear to be slightly more stable than NV-VLP alone because at low temperatures the tryptophan peak position is around 339 nm (Figure 10B). In the presence of alhydrogel, however, there was no significant change in the Tm values, in the presence of excipients (10% sucrose, 15% mannitol and a combination of both) although the VLP seems to be better stabilized as evident from the shift in Tm to higher temperatures around 69^{o}C.

Conclusion:

Aluminum hydroxide particles possess needle-like or fibril morphology, with a diameter of approximately 2 mm with a high surface area.[58,59] The large surface area provides excellent adsorptive capability for protein antigens. Electrostatic forces often play a dominant role during alhydrogel binding to proteins although hydrophobic interactions also partially contribute to the adsorption of proteins to aluminum hydroxide gel. The pI of Consensus G11.4 VLP is 5.61 and that for NV-VLP is 5.64. Thus both the VLPs tend to bind to alhydrogel which is a basic salt particulate, presumably involving electrostatic forces at least to some extent. NV-VLP seems to be better stabilized in the

presence of alhydrogel alone compared to Consensus G11.4 VLP as evident from an increase in its melting temperature by 4^{o}C. In the presence of excipients, the melting temperature for the adsorbed NV-VLP does not change to a detectable extent. In contrast, the Consensus G11.4 VLP shows better stability in the presence of excipients when adsorbed to Alhydrogel.

References:

1. Black RE, Cousens S, Johnson HL, Lawn JE, Rudan I, Bassani DG. (2010) Global, regional, and national causes of child mortality in 2008: a systematic analysis. *Lancet* 5 375(9730):1969-87.
2. Liu L, Johnson HL, Cousens S, Perin J, Scott S, Lawn JE, Rudan I, Campbell H, Cibulskis R, Li M, Mathers C, Black RE (2012) Child Health Epidemiology Reference Group of WHO and UNICEF. Lancet. Jun 9;379(9832):2151-61.
3. GBD Causes of Death Mortality Collaborators,*Global, regional, and national age-sex specific all- cause and cause-specific mortality for 240 causes of death, 1990-2013: a systematic analysis for the Global Burden of Disease Study 2013.* Lancet, 2015. 385(9963): p. 117-71.
4. Liu, L., et al., *Global, regional, and national causes of child mortality in 2000-13, with projections to inform post-2015 priorities: an updated systematic analysis.* Lancet, 2015. 385(9966): p. 430-40.
5. Global Burden of Disease Study Collaborators, *Global, regional, and national incidence, prevalence, and years lived with disability for 301 acute and chronic diseases and injuries in 188 countries, 1990-2013: a systematic analysis for the Global Burden of Disease Study 2013.* Lancet, 2015.
6. Glass RI, Kilgore PE. Etiology of acute viral gastroenteritis. In: Gracey M, Walker JA, eds. Diarrheal disease. NestleÂ Nutrition Workshop Series. Philadelphia: Lippincott-Raven, 1997: 39±54.
7. Christensen ML. Rotaviruses. In: Murray PR, Baron EJ, Pfaller MA, Tenover FC, Yolken RH, eds. Manual of clinical microbiology. Washington: ASM Press, 1999: 999±1004.
8. Medical Microbiology: a guide to microbial infection: pathogenesis, immunity, laboratory diagnosis and control. 17th edition p.659-660.
9. Hall AJ, Wikswo ME, Manikonda K, Roberts VA, Yoder JS, Gould LH (2013). Acute gastroenteritis surveillance through the National Outbreak Reporting System, United States. Emerg Infect Dis.
10. Payne DC, Vinjé J, Szilagyi PG, Edwards KM, Staat MA, Weinberg GA, Hall CB, Chappell J, Bernstein DI, Curns AT, Wikswo Mary, Shirley SH, Hall AJ, Lopman B, Parashar UD (2013) Norovirus and Medically Attended Gastroenteritis in U.S. Children. N Engl J Med 368:1121-1130.
11. *Tate JE, Cortese MM, Payne, DC, et al. (2011) Uptake, impact, and effectiveness of rotavirus vaccination in the United States: review of the first 3 years of postlicensure data. Pediatr Infect Dis J 30: S56 - S60*
12. Tate JE, Mutuc JD, Panozzo CA, et al (2011) Sustained decline in rotavirus detections in the United States following the introduction of rotavirus vaccine in 2006. Pediatr Infect Dis J 30: S30 - S34.
13. Clark B, McKendrick M (2004). A review of viral gastroenteritis. Curr Opin Infect Dis 17(5):461-9.
14. Ahmed SM, Hall AJ, Robinson AE, Verhoef L, Premkumar P, Parashar UD, Koopmans M, Lopman BA (2014). Global prevalence of norovirus in cases of gastroenteritis: a systematic review and meta-analysis. Lancet Infect Dis 14(8):725-30.
15. Adler JL, Zickl R (1969). Winter vomiting disease. J. Infect. Dis. 119:668-673
16. Kapikian AZ, Wyatt RG, Dolin R, Thornhill TS, Kalica AR, Chanock RM (1972) Visualization by immune electron microscopy of a 27-nm particle associated with acute infectious nonbacterial gastroenteritis. J Virol 10:1075–81.
17. Xi JN, Graham DY, Wang KN, Estes MK (1990) Norwalk virus genome cloning and characterization. Science 14;250(4987):1580-3.

18. Kapikian AZ, Wyatt RG, Dolin R, Thornhill TS, Kalica AR, Chanock RM (1972) Visualization by immune electron microscopy of a 27-nm particle associated with acute infectious nonbacterial gastroenteritis. J Virol 10(5):1075-81.
19. Hardy ME, Estes MK (1996) Completion of the norwalk viruse genome sequence. Virus genes 12:289-292
20. Jiang et al (1993) Sequence and genomic organization of norwalk virus. virology 195:51-61
21. Matsui et al (1991) The isolation and and charecterization of norwalk virus specific cDNA. J clin investig 87:1456-1461
22. Zheng DP, Ando T, Fankhauser RL, Beard RS, Glass RI, Monroe SS (2006) Norovirus classification and proposed strain nomenclature. Virology 346:312–23.
23. Bertolotti-Ciarlet A, Crawford SE, Hutson AM, Estes MK (2003) The 3' end of Norwalk virus mRNA contains determinants that regulate the expression and stability of the viral capsid protein VP1: a novel function for the VP2 protein. J Virol 77 (21): 11603-15.
24. Wang QH, Han MG, Cheetham S, Souza M, Funk JA, Saif LJ (2005) Porcine noroviruses related to human noroviruses. Emerg Infect Dis 11:1874–81.
25. Siebenga JJ, Vennema H, Zheng DP, et al. (2009) Norovirus illness is a global problem: emergence and spread of Norovirus GII.4 Variants, 2001–2007. J Infect Dis 200:802–12.
26. Lindesmith LC, Donaldson EF, Lobue AD, et al. (2008) Mechanisms of GII.4norovirus persistence in human populations. PLoS Med 5: e31.
27. Hutson AM, Atmar RL, Estes MK (2004). Norovirus disease: changing epidemiology and host susceptibility factors. Trends Microbiol 12:279–287
28. Chakravarty S, Hutson AM, Estes MK, Prasad BV (2005) Evolutionary trace residues in noroviruses: importance in receptor binding, antigenicity, virion assembly, and strain diversity. J Virol 79:554–568.
29. Cannon JL, Lindesmith LC, Donaldson EF, Saxe L, Baric RS, Vinjé J (2009) Herd immunity to GII.4 noroviruses is supported by outbreak patient sera. J Virol 83:5363-5374.
30. Chen R, Neill JD, Estes MK, Venkataram Prasad BV (2006) X-ray structure of a native calicivirus: Structural insights into antigenic diversity and host specificity. PNAS 103: 8048-8053.
31. Parra GI, Bok K, Taylor R, Haynes JR, Sosnovtsev SV, Richardson C, Green KY (2012) Immunogenicity and specificity of norovirus Consensus GII.4 virus-like particles in monovalent and bivalent vaccine formulations. Vaccine 21 30(24):3580-6.
32. Kueltzo LA, Ersoy B, Ralston JP, Middaugh CR (2003) Derivative absorbance spectroscopy and protein phase diagrams as tools for comprehensive protein characterization: a bGCSF case study. J Pharm Sci 92 (9): 1805-20.
33. Ausar SF, Espina M, Brock J, Thyagarayapuran N, Repetto R, Khandke L, Middaugh CR (2007) High-throughput screening of stabilizers for respiratory syncytial virus: identification of stabilizers and their effects on the conformational thermostability of viral particles. Hum Vaccin 3 (3): 94-103.
34. Srimathi T, Kumar TK, Kathir KM, Chi YH, Srisailam S, Lin WY, Chiu IM, Yu C (2003) Structurally homologous all beta-barrel proteins adopt different mechanisms of folding. Biophys J 85:459–472.
35. Manning MC, Illangasekare M, Woody RW (1988) Circular dichroism studies of distorted alpha-helices, twisted beta-sheets, and beta turns. Biophys Chem 31: 77–86.
36. Khan MY, Villanueva G, Newman SA (1989) On the origin of the positive band in the far-ultraviolet circular dichroic spectrum of fibronectin. J Biol Chem 264: 2139–2142.
37. Perczel A, and Fasman GD (1992) Quantitative analysis of cyclic βturn models. Protein Science I, 378-395.

38. Ausar SF, Foubert TR, Hudson MH, Vedvick TS, Middaugh CR (2006). Conformational stability and disassembly of Norwalk virus-like particles. Effect of pH and temperature. J. Biol. Chem. 281:19478 –19488.
39. White LJ, Hardy ME, Estes MK (1997) Biochemical characterization of a smaller form of recombinant Norwalk virus capsids assembled in insect cells. J Virol 71, 8066-8072.
40. Kissmann J. Ausar SF, Foubert TR, Brock J, Switzer MH, Detzi EJ, Vedvick TS, Middaugh CR (2008). Physical Stabilization of Norwalk Virus-like Particles. J Pharm Sci. 97:4208–4218.
41. Lentzen G. Schwarz T. (2006). Extermolytes: natural compounds from extermopliles for versatile applications. Appl. Microbiol. Biotechnol. 72: 623-634.
42. Kumar R. (2009). Role of naturally occurring osmolytes in protein folding and stability. Arch. Biochem. Biophys. 491:1-6
43. Ausar, S. F.; Espina, M.; Brock, J.; Thyagarayapuran, N.; Repetto, R.; Khandke, L.; Middaugh, C. R., High-throughput screening of stabilizers for respiratory syncytial virus: identification of stabilizers and their effects on the conformational thermostability of viral particles. *Hum Vaccin* **2007,** 3, (3), 94-103.
44. Peek, L. J.; Brandau, D. T.; Jones, L. S.; Joshi, S. B.; Middaugh, C. R., A systematic approach to stabilizing EBA-175 RII-NG for use as a malaria vaccine. *Vaccine* **2006,** 24, (31-32), 5839-51.
45. Kaushik JK. Bhat R. (2003). Why terhalose an exceptional protein stabilizer? An analysis of the thermal stability of proteins in the presence of the compatible osmolyte terhalose. J. Biol. Chem. 278:26458-26465.
46. Johnson RE. Kirchhoff CF. Gaud HT. (2002). Mannitol-sucrose mixture-versatile formulations for protein lyophilization. J. Pharm. Sci. 91:914-922.
47. Glenny AT, Pope CG, Waddington H, Wallace V. (1926). The antigenic value of toxoid precipitated by potassium-alum. J Path Bact 29:38-45.
48. Allison AC, Byars NE. (1991). Immunological adjuvants: desirable properties and side-effects. Mol Immunol 28:279-84.
49. Glenny AT, Buttle GAH, Stevens MF. (1931) Rate of disappearance of diphtheria toxoid injected into rabbits and guinea-pigs: toxoid precipitation with alum. J Pathol Bacteriol. 34:267-287.
50. Grun JL, Maurer PH. (1989). Different T helper cell subsets elicited in mice utilizing two different adjuvants vehicles: the role of endogenous interleukin 1 in proliferative response. Cell Immunol. 121:134-145.
51. Kool M, et al. (2008) Alum adjuvants boosts adaptive immunity by introducing uric acid and activating inflammatory dendritic cells. J Exp Med. 205:869-882.
52. Kono H, Rock KL. (2008). How dying cells alert the immune system to danger. Nature Rev Immunol. 8:279-289.
53. Vogel FR, Powell MF. (1995). A compendium of vaccine adjuvants and excipients. Pharm. Biotechnol. 6: 141-228.
54. Berthold I, Pombo ML, Wagner L, Arciniega JL. (2005). Immunogenicity in mice of anthrax recombinant protective antigen in the presence of aluminum adjuvants. Vaccine. 23:1993-1999.
55. Romero Mendez IZ, Shi Y, HogenEsch H, Hem SL. (2007). Potentiation of the immune response to non-adsorbed antigens by aluminum-containing adjuvants. Vaccine 25:825-833.
56. al-Shakhshir RH, Regnier FE, White JL, Hem SL. (1995). Contribution of electrostatic and hydrophobic interactions to the adsorption of proteins by aluminum-containing adjuvants. Vaccine. 13:41-44.
57. Peek LJ, Martin TT, Elk Nation C, Pegram SA, Middaugh CR. (2007). Effects of stabilizers on the destabilization of proteins upon adsorption to aluminum salt adjuvants. J Pharm Sci. 96(3):547-57.
58. Shirodkar S, Hutchinson RL, Perry DL, White JL, Hem SL. (1990). Aluminum compounds used as adjuvants in vaccines. Pharm. Res. 7: 1282–1288.

59. Kubicki JD, Apitz SE. (1998) Molecular cluster models of aluminum oxide and aluminum hydroxide surfaces. Am. Mineral. 83:1054–1066.

Tables

Table 1: Transition midpoint (Tm) values for Consensus G11.4 VLP at different pH values obtained from the changes in the CD melts of consensus VLP as a function of temperature (n=2).

pH	Tm(C°) ± SD
3	72.23 ± 0.37
4	74.72 ± 0.66
5	74.87 ± 0.31
6	78.52 ± 0.57
7	indecisive
8	indecisive

Table 2: Transition midpoint (Tm) values for Consensus G11.4 VLP at different pH values obtained from the changes in the tryptophan emission fluorescence as a function of temperature. (n=2)

pH	Tm(°C)±S.D.
3	54.6 ±0.36
4	61.5±0.64
5	64.6 ±0.45
6	64.8±0.38
7	61.2±0.25
8	57.0±0.28

Table 3: Onset Temperature of aggregation (T_{onset}) values for Consensus G11.4 VLP at different pH values obtained from static light scattering data (n=2).

pH	**T_{onset} (C°)**
3	55
4	58
5	56
6	62
7	60
8	53

Table 4: Percentage inhibition of aggregation of consensus G11.4 VLP in the absence and presence of different excipients. Compounds, which inhibit aggregation, have positive % of aggregation values and those, which accelerate aggregation, have negative % of aggregation values. The average % error is of the order of ±5%.

Consensus VLP ± Excipients	**Concentration**	**%Inhibition of Aggregation**
Consensus VLP only	0.1 mg/ml	100
+Sodium Citrate	0.2M	100
+Trehalose	20%	100
+Dextrose	20%	100
+Glycerol	15%	98
+Lysine	0.3M	94
+Sucrose	20%	91
+Mannitol	10%	90
+Treh 15%	15%	87
+Treh 10%	10%	86
+Glutamic Acid	0.15	86
+Sorbitol	20%	82
+sod cit 0.1M	0.1M	76
+sod cit 0.05M	0.05M	74
+Glycerol 10%	10%	74
+Glycine	0.3M	71
+Malic Acid	0.15M	66
+Proline	0.3M	62
+2-OH propyl g-CD	10%	57
+Arginine	0.3M	53
+Lactose	20%	52

+2-OH propyl g-CD	5.00%	28
+Arginine	0.15M	26
+Aspartic Acid	0.075M	24
+2-OH propyl b-CD	10%	21
+Glutamic Acid	0.05M	16
+Glutamic Acid	0.1M	7
+Calcium Chloride	0.015M	7
+Arginine	0.1M	1
+Dietanolamine	0.3M	-4
+Brij 35 30% (w/v)	0.10%	-5
+g-CD	2.50%	-7
+Lys 0.1 M	0.1M	-7
+Lactic Acid 85%	0.15M	-11
+Lys 0.15M	0.15M	-13
+a Cyclodextrin	2.5%	-14
+Histidine	0.3M	-18
+Tween 20	0.10%	-26
+Tween 80	0.10%	-28
+Guanidine-HCl	0.3M	-32
+Pluronic F-68	0.10%	-32
+Dextran Sulfate	0.0075 mM	-76
+Gelatin	5.0%	na
+Ascorbic acid	0.15M	na
+Albumin	5%	na

Table 5: Transition midpoints (T_m) and shifts in the T_m values observed for Consensus G11.4 VLP in presence of selected combinations and concentrations of excipients (n=2).

Excipients	Tm(°C)	Tm Shfit (°C)
None	65.44±0.11	None
+15%Treh	65.61±0.10	None
+15%glycerol	65.6±0.14	None
+10%gly+10%treh	65.37±0.12	None
+0.3M arg	62.84±0.20	-2.60
+20%mannitol	68.35±0.09	+2.91
+15%mannitol	67.83±0.081	+2.39
+20%sucrose	67.47±0.12	+2.03
+15%suc	67.16±0.12	+1.72
+10%man+10%suc	67.92±0.08	+2.48
+10%man+15%suc	67.88±0.09	+2.44
+10%suc	66.12±0.12	+0.68
+10%man	67.14±0.14	+1.7
+10%suc+15%man	69.72±0.13	+4.28
+5%suc+5%man	65.93±0.11	+0.49
+10%suc+5%man	67.44±0.13	+2
+5%suc+10%man	67.16±0.15	+1.72

Table 6: Average T_m (midpoint of transition) values of norovirus VLPs in solution and when adsorbed to alhydrogel in absence and presence of stabilizers. (n=2). Tm values are determined by using the non-linear curve fit program of Origin 7.0 software.

Virus-like Particle	Adjuvant (+/- excipients)	Tm (ºC)±S.D.
NV-VLP	Without alhydrogel	64.0ºC±0.34
	With alhydrogel	68.2ºC±0.14
	With alhydrogel+10% sucrose	68.7ºC±0.23
	With alhydrogel+15% mannitol	68.25ºC±0.23
	With alhydogel+10%sucrose+15% mannitol	69.9ºC±0.21
Consensus G11.4 VLP	Without alhydrogel	63.98ºC±0.49
	With alhydrogel	63.79ºC±0.26
	With alhydrogel+10%sucrose	69.18ºC±0.16
	With alhydrogel+15%mannitol	69.81ºC±0.16
	With alhydrogel+10%sucrose+15%mannitol	69.16ºC±0.21

Figures

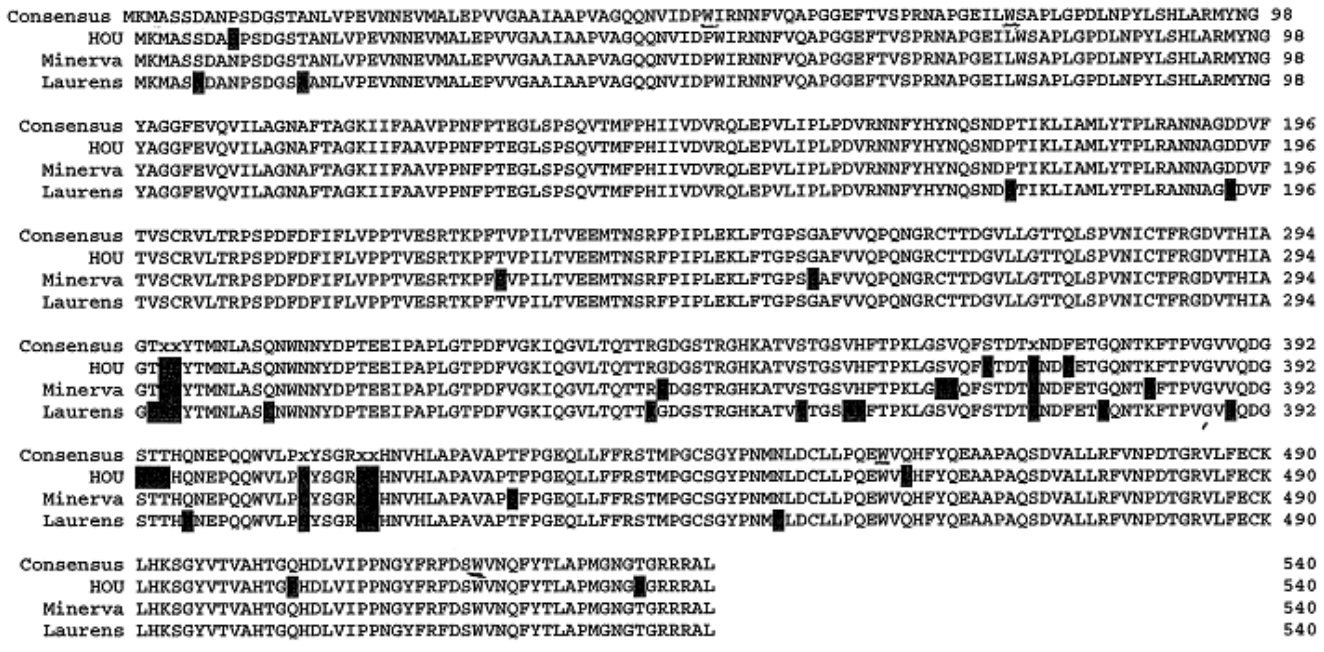

Figure 1: Sequence analysis of Consensus G11.4 VLP with Houston G11.4 strain and two 2007 G11.4 strains.

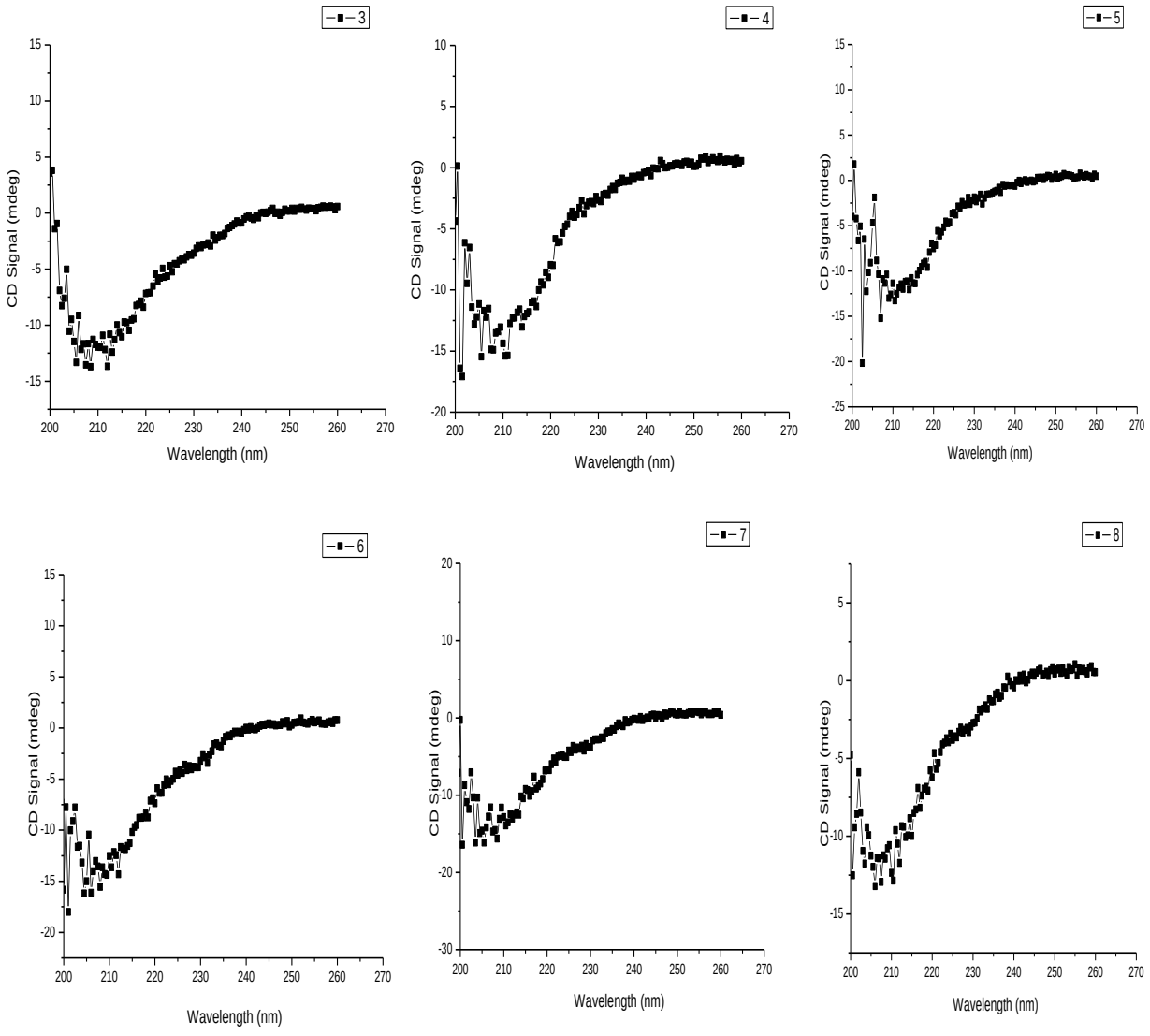

Figure 2: (A) CD Spectra of consensus G11.4 VLPs plotted individually at 10ºC at different pH values.

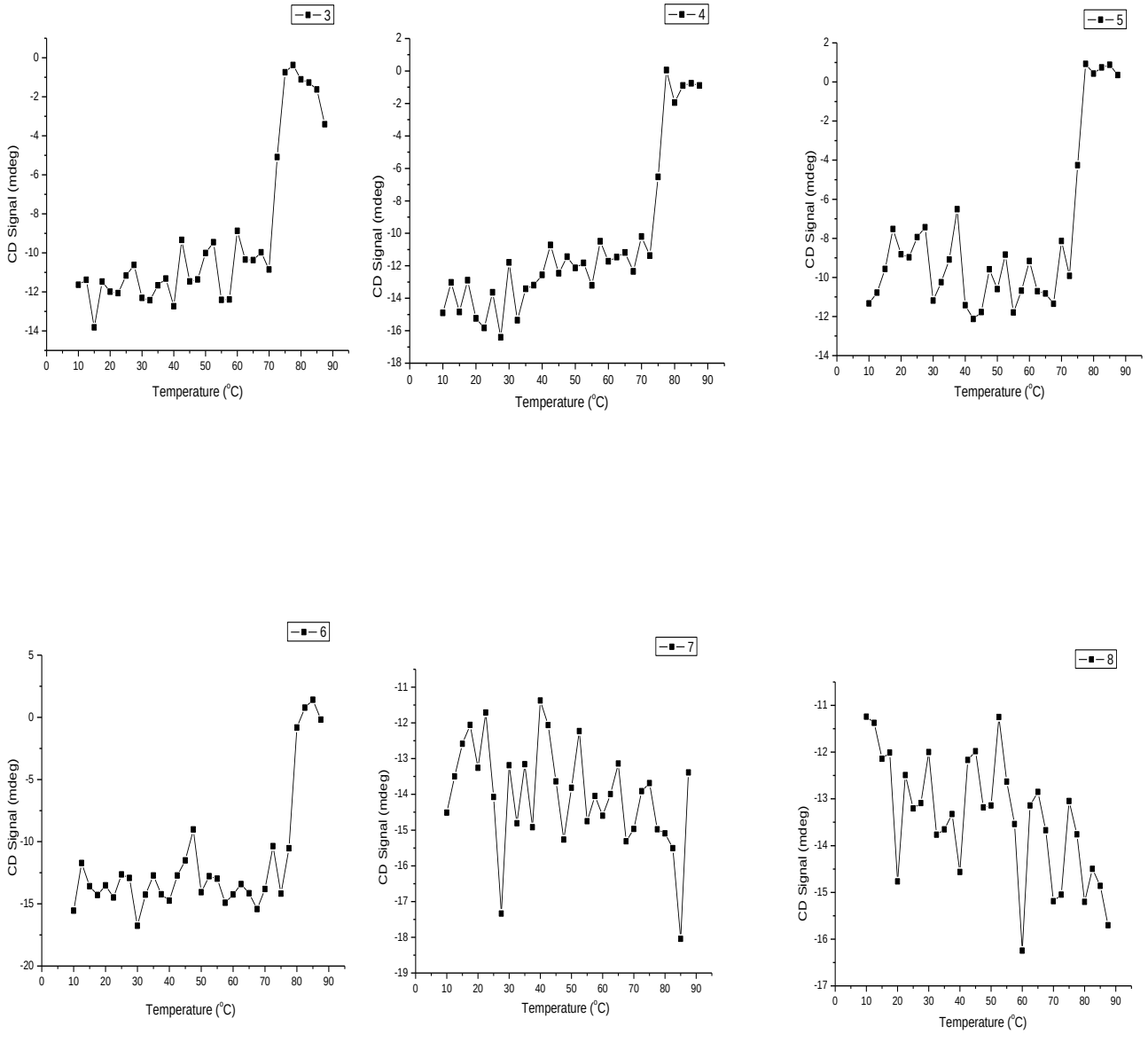

Figure 2 (B): CD melts of consensus VLP at different pH values (n=2)

A

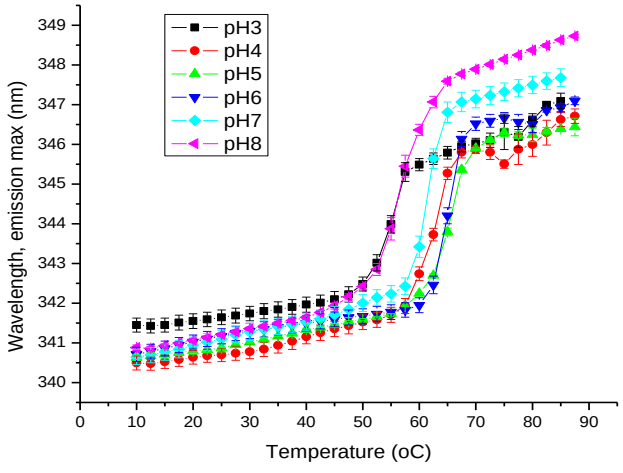

B

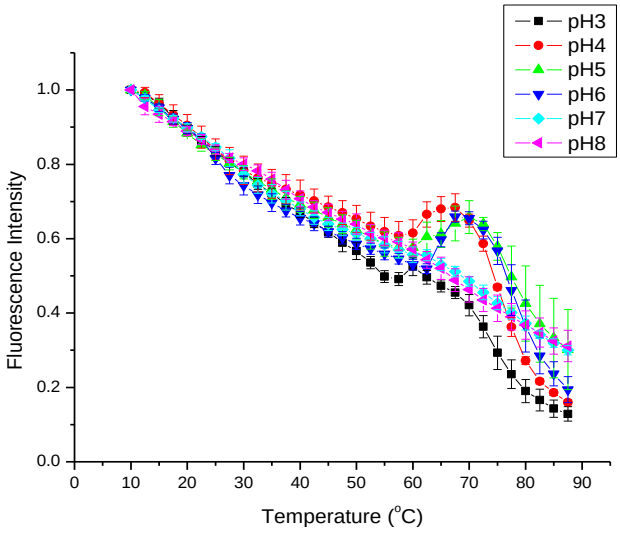

Figure 3:

A) Tryptophan peak position changes of consensus VLP as a function of pH and temperature (n=2).
B) Tryptophan Fluorescence Intensity changes of Consensus VLP as a function of pH and temperature (n=2).

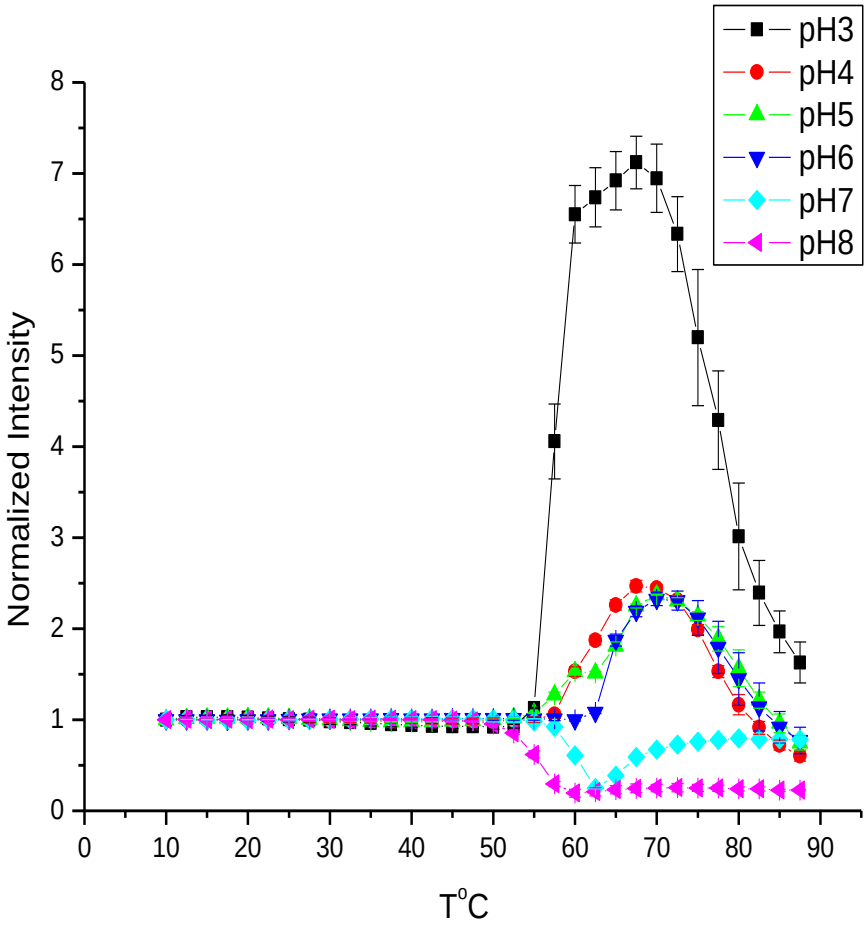

Figure 4: Static Light Scattering of consensus VLP as a function of pH and temperature (n=2).

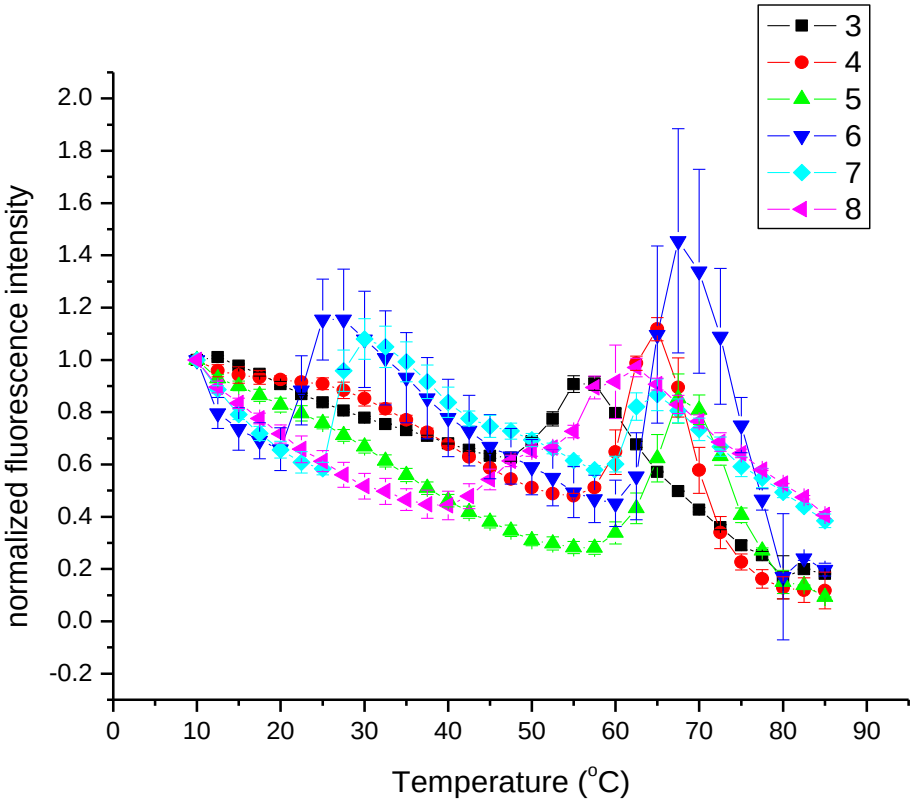

Figure 5: ANS extrinsic fluorescence intensity changes of the Consensus G11.4 VLP as a function of pH and temperature (n=2).

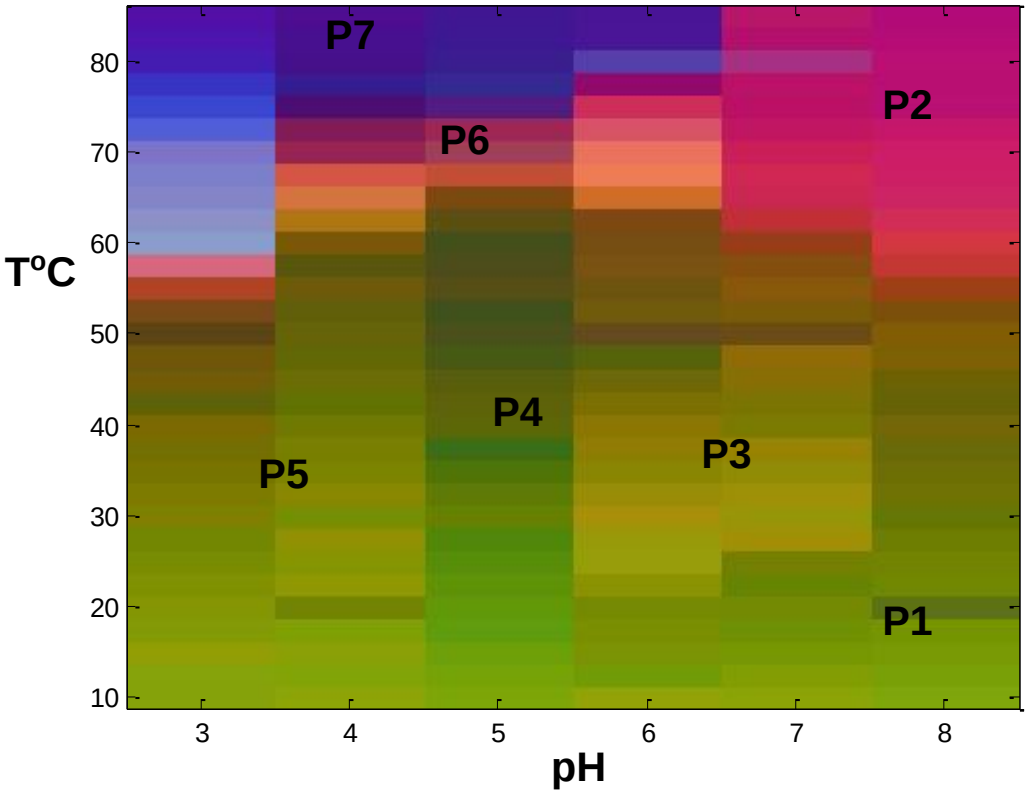

Figure 6: *Empirical Phase Diagram of Consensus G11.4 VLP based on data from circular dichroism, tryptophan peak position changes, trytophan fluorescence intensity changes, ANS fluorescence intensity changes and static light scattering*.

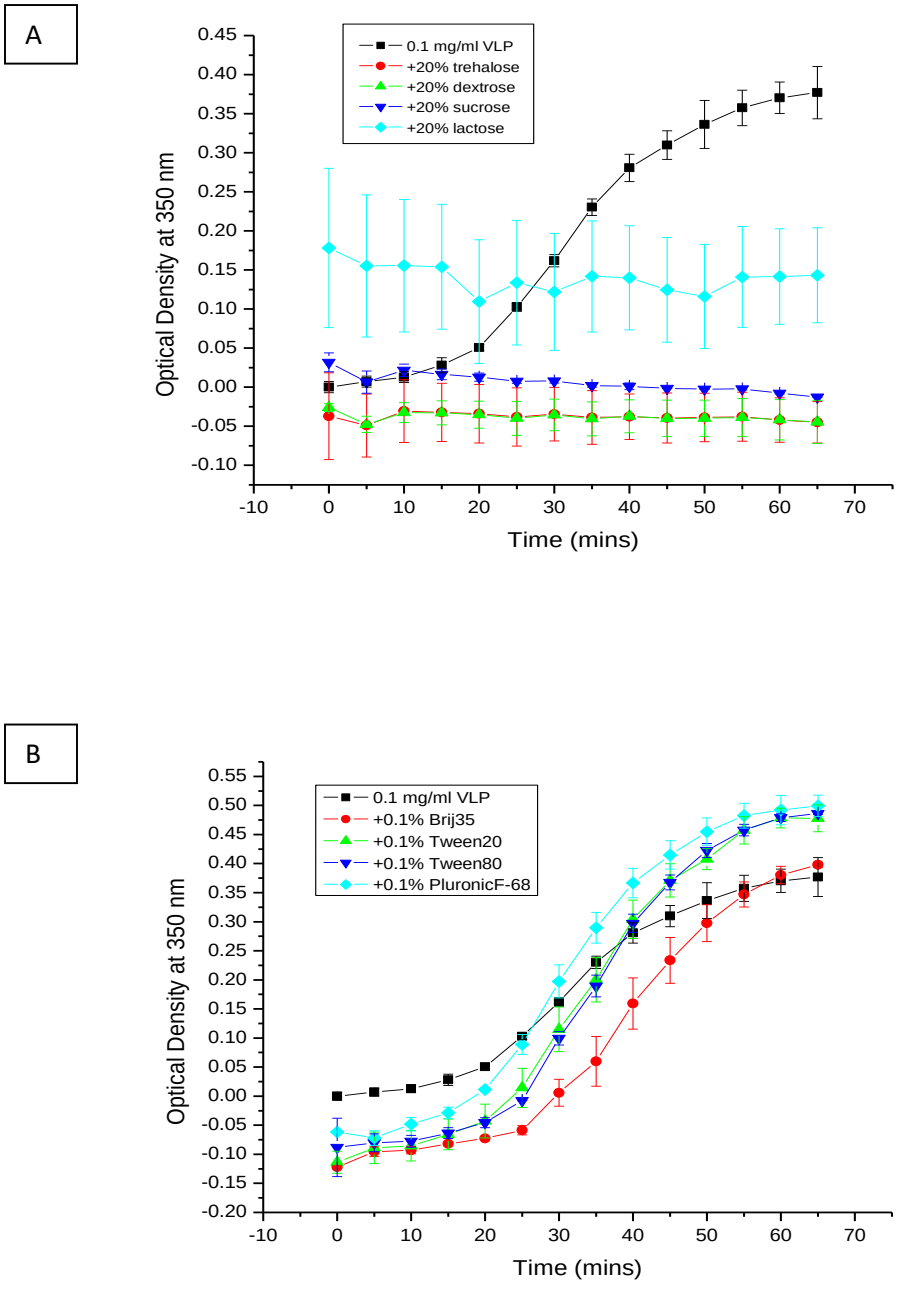

Figure 7: Aggregation kinetics of Consensus G11.4 VLP in the presence of selected excipients. VLP (0.1 mg/ml) in 20mM isotonic citrate phosphate buffer, pH 5.0 was incubated in the presence and absence of excipients at 60°C for 1 hour and the scattering intensity was monitored by measuring the optical density (OD at 350nm) every 5 min.(n=2) (A)VLP+excipients which inhibit the aggregation of VLP (B) VLP+excipients which do not inhibit aggregation of VLP

A

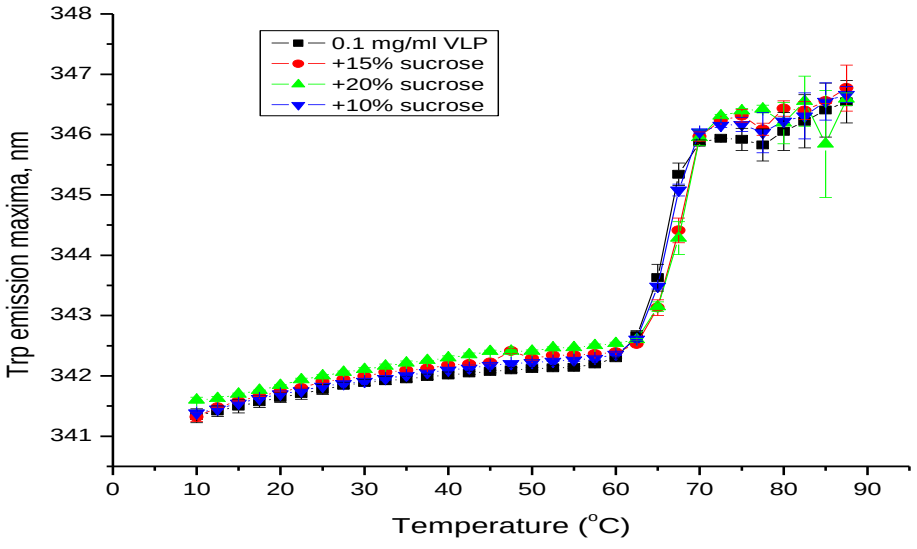

B

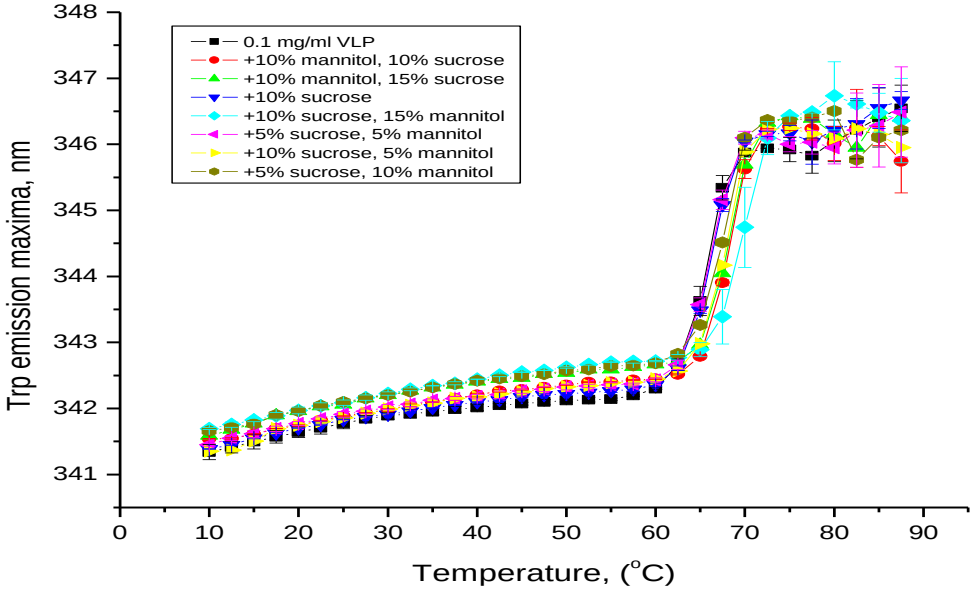

Figure 8(A, B): Tryptophan emission peak position as a function of pH and temperature. VLP solutions in the presence of selected excipients in 20 mM Histidine buffer, pH 6.5+0.15M NaCl were heated from 10 to 85 °C, and the fluorescence emission maxima were monitored upon excitation at 295 nm(n=2).

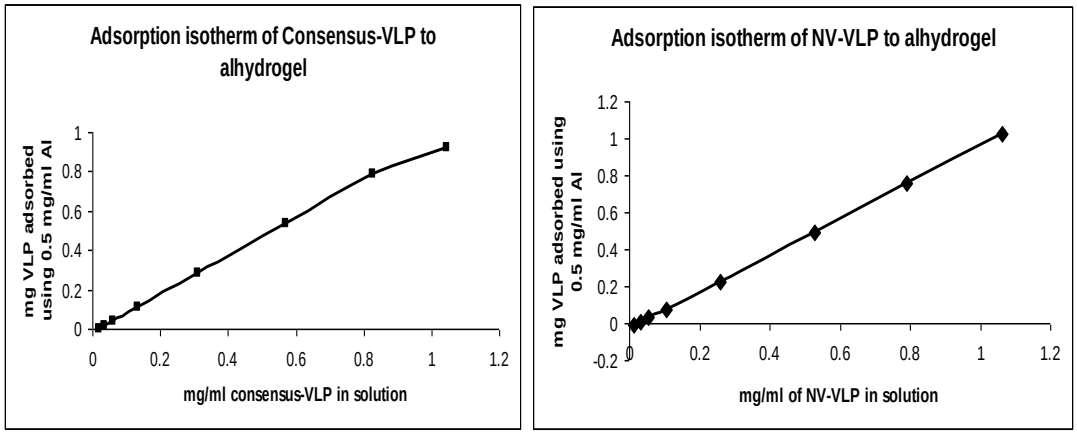

Figure 9A: Binding isotherms of Consensus G11.4 VLP and NV-VLP to Alhydrogel

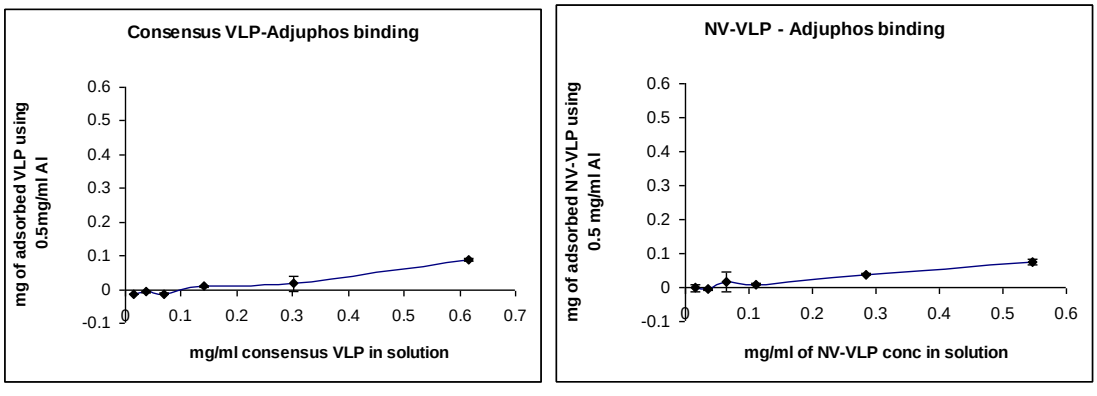

Figure 9B: Binding isotherms of Consensus G11.4 VLP and NV-VLP to Adjuphos.

A

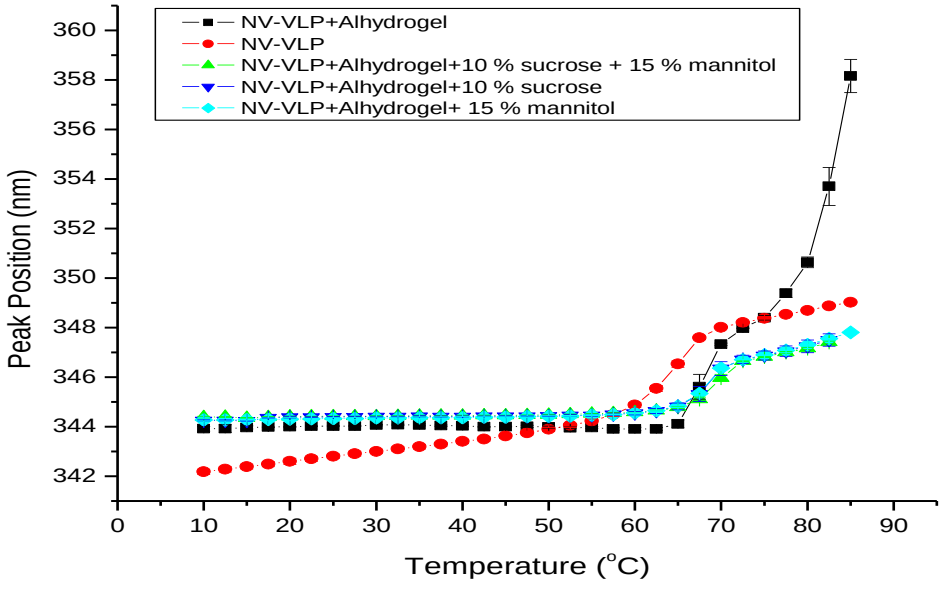

Figure 10(A): Tryptophan peak position changes determined by front face fluorescence spectroscopy for NV-VLP in solution and when adsorbed to alhydrogel in the absence and presence of selected excipients.

B

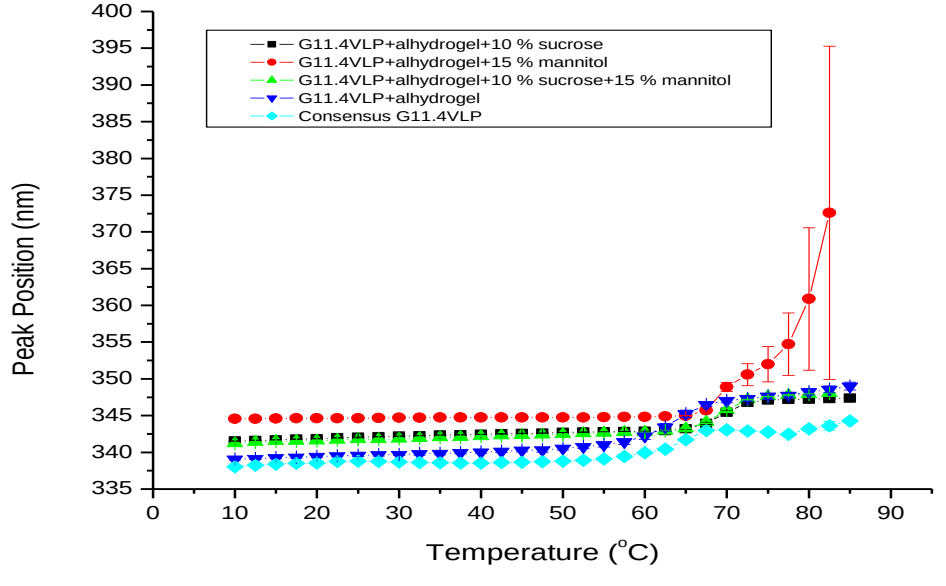

Figure 10(B): Tryptophan peak position changes determined by front face fluorescence spectroscopy for Consensus G11.4-VLP in solution and when adsorbed to alhydrogel in the absence and presence of selected excipients.